Available online at www.sciencedirect.com

ScienceDirect

Materials Today: Proceedings 00 (2014) 000–000

materialstoday: PROCEEDINGS

www.materialstoday.com/proceedings

5th International conference on Advanced Nano Materials

The current crowding effect in ZnO nanowires with a metal contact

O. Kryvchenkova[a]*, R. J. Cobley[a], K. Kalna[b]

[a]*Multidisciplinary Nanotechnology/*[b]*Electronic Systems Design Centre Centre, College of Engineering, Swansea University, Singleton Park, Swansea, SA2 8PP, Wales, United Kingdom*

Abstract

Nanoscale electron tunneling and thermionic transport via the metal-semiconductor interface of ZnO nanowires is found to be strongly affected by the metal contact shape, the metal-semiconductor interface radius and the nanowire radius. Our full 3D simulations show that the current crowding effect occurs for end-bonded contacts due to the geometry variation in the case of Schottky Au-ZnO nanowire interfaces. The change in the geometry will also lead to a change in the electrical behavior of the contact from Schottky to Ohmic which can substantially reduce the contact resistance.

Keywords: nanowires; current crowding; tunnelling;

Introduction

The transport properties of metal nanocontacts fabricated for various nanostructure devices[1–3] have become to be recognized as a major challenge to device functionality. Attention has been drawn to their geometrical properties[4,5], since the repeatable manufacture is still challenging and transport at the nanoscale is poorly understood. Out of these nanostructures, ZnO nanowires (NWs) have been intensively studied for potential applications including Schottky diodes, ZnO NW FETs for displays, gas and medical sensors, and UV NW photodetectors[6]. ZnO nanowires fabricated using a catalyst[7] are excellent candidates for the study of the geometrical and transport properties via the Au-ZnO interface due to low solubility of the solid catalyst material in the NW during and after growth[8–10].

In this work, we investigate electron transport through the nanoscale Au-ZnO interface using the full 3D device simulator tool ATLAS by Silvaco[11] as a function NW radius. We have found that current crowding in ZnO NWs plays an essential role by increasing parasitic resistance at the edge of the downscaled contacts. The parasitic resistance will lead to a local temperature rise at the metal-semiconductor interface[1]. Generally, there are two main classes of nanowire contact geometries: side-bonded contacts which are produced when metal contacts are deposited on to nanostructures, and end-bonded contacts which normally have an intimate metal contact at the top of the nanowire[5]. The current crowding effect was reported earlier in side-bonded nanostructures like carbon nanotubes[2,12], ZnO, GaN and Si nanowires[13], and graphene-metal contacts[3]. Using a 1D electrothermal model, LeBlanc *et al* [13] demonstrated that for ZnO NWs with side-bonded Ohmic contacts, the peak of the temperature rise will occur at the metal-nanowire interface. Post-measurement images of the ZnO NW with side-bonded Ti/Ag contacts indicated melting of the metal electrode, limiting the operational range of these devices. We investigate the current crowding effect in end-bonded contacts in relation to the change in NW radius for the ZnO-Au Schottky interface using 3D real space simulations. The simulations demonstrate that using lower dimension calculations in 2D will give a different effect, while the contact phenomena cannot be studied using a 1D modeling.

Unlike microscale contacts, where the ability to select between Ohmic and Schottky behavior is performed by selecting a metal with appropriate workfunction and semiconductor material properties, nanoscale contacts do not follow a bulk properties of the material[14,15]. The transport properties of the nanocontact will depend on the size and geometry of the contact but there is still no generalized understanding of these effects in the literature[5,16,17].

2. Simulation method

2.1. Geometry and material parameters

Transmission electron microscopy (TEM) images of the ZnO-Au structure[7] indicate a complex shape of the Au particle standing on top of the nanowires of various radius. To have a good geometrical representation of the

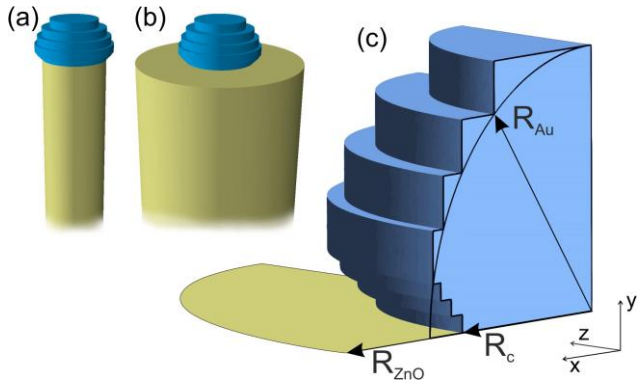

Fig. 1. 3D simulations of ZnO NWs with Au particle (R_{Au}=15 nm) deposited on the top and forming the contact radii R_c=12 nm with (a) R_{ZnO}=12 nm and (b) R_{ZnO}=30 radii of ZnO NWs. The length of the ZnO NW is 900 nm so only the top ~70 nm of the structure is shown here. (c) Approximation of the shape of a gold particle.

structure in the simulations, we mimic the shape from images of the Au particle where the interface radius is 80-90% smaller than the Au particle radius[7]. Figs. 1(a) and (b) illustrate such structures with different ZnO NW radii for the gold particle radius of R_{Au}=15 nm. In the structure shown in Fig. 1(a), the ZnO NW radius is equal to the metal-semiconductor interface radius of R_c=12 nm. In the structure in Fig. 1(b), a ZnO NW has a radius of R_{ZnO}=30 nm and nanowire radius is significantly larger than the metal-semiconductor interface area. The NW length of 900 nm was assumed in all simulations. A 15 nm radius of the Au particle was approximated using 4 large cylindrical layers. An 80% change in the particle at the base of the contact was approximated using 3 cylindrical sublayers (Fig. 1(c)).

The following material parameters were used for ZnO[18]: band gap (E_g) 3.37 eV, electron affinity (χ) 4.5 eV, and *n*-type doping of 10^{18} cm^{-3} assuming a gold work function (ϕ_m) of 5.1 eV. The interface charge at the NW surface and at the contact interface is neglected to study purely the influence of the geometry variations.

2.2. Model

The work function of 5.1 eV for the Au creates a 0.6 eV potential barrier (ϕ_b) at the interface as calculated from the standard expression of the Schottky-Mott theory $\phi_m=\chi+\phi_b$ [14]. Note here that additional barrier lowering due to the image force effect and the dipole effect are accounted for in the simulations[19].

The surface potential ψ_s changes with the applied voltage, *V*, and depends on the conduction (N_C) and valence (N_V) band density of states as:

$$\psi_S = \frac{kT}{2q}\cdot\ln\left(\frac{N_C}{N_V}\right)-\phi_m+\chi+V \qquad (1)$$

The electric field is taken into calculations of the surface recombination velocities where the image force effect and dipole effect were taken into account in the calculation of the potential barrier. All quantities are calculated at each element of the triangular mesh of the structure. The thermionic emission current is calculated for both electrons and holes using a surface concentration of electrons (holes), n_s (p_s), and equilibrium concentration of electrons (holes), *n* (*p*). The equation for electrons (holes) is defined as[20]:

$$J = q\frac{AT^2}{qN_C}\left(n_s-n\right)\exp\left(\Delta\phi_b/kT\right) \qquad (2)$$

with a respective replacement of n_s to p_s and *n* to *p* for holes. The universal Schottky tunneling model [21,22] is used to calculate the tunneling current J_{tunn} between semiconductor and metal. The tunneling current accounts for the localized tunneling rates $G_T=1/q\cdot\nabla J_{tunn}$ at every grid point of the semiconductor region for both electrons and holes up to 10^{-6} cm from the conductor:

$$J_{tunn} = \frac{AT}{k}\int_0^\infty \Gamma(E)\ln\left(\frac{1+f_{ZnO}(E)}{1+f_{Au}(E)}\right)dE \qquad (3)$$

where *A* is the effective Richardson's coefficient, $\Gamma(E)$ tunneling probability, $f_{ZnO}(E)$ and $f_{Au}(E)$ are Maxwell-Boltzmann distribution functions in the ZnO semiconductor and Au[23].

The tunneling current through the air gap was calculated using a direct quantum tunneling model[24]. The results have shown that tunneling through the air gap is at least 4 orders of magnitude smaller than the current through the contact area so that the tunneling via air gap can be neglected in the simulations. Finally, Dirichlet boundary conditions are used for contacts and homogeneous (reflecting) Neumann boundary conditions are used for the non-contact areas.

3. The Effect of Current Crowding

The current crowding effect, that leads to the non-uniform distribution of the current density near the edge of the metal contact was reported earlier for nanostructures like silicon MOSFETs[1], carbon-nanotubes with side contacts[2], graphene sheets[3], and other side-bonded contacts and structures lying flat on the substrate. In the present work, we focus on the size-dependent effect of current crowding in end-bonded contacts for the ZnO NW

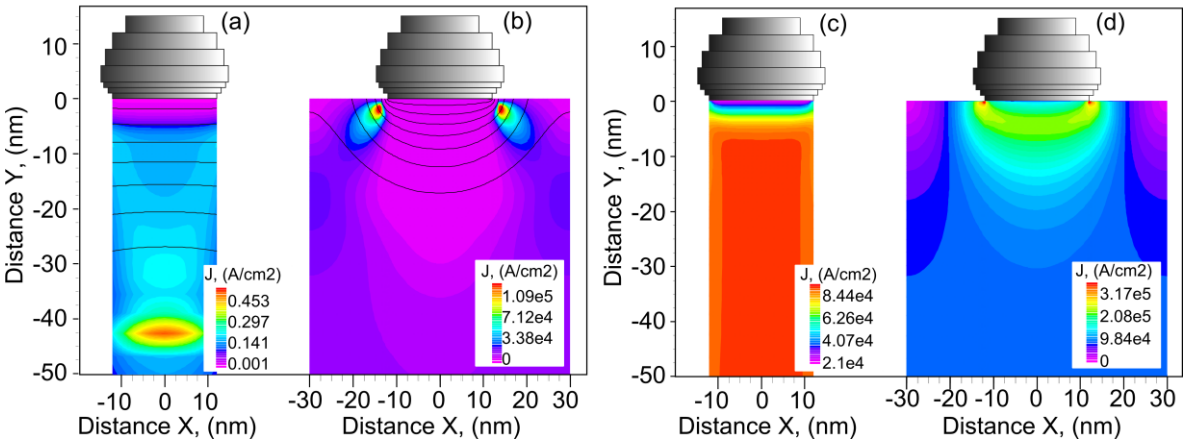

Fig. 2. The spatial distribution of the current density for −1 V (a, b) and +1 V (c, d) indicates a size-dependent current crowding effect. Black solid lines in (a) and (b) show a potential distribution under the metal contact, indicating a size-dependent effect of the depletion width.

structure. In Fig. 2, the spatial current density distribution for the bias of −1 V and +1 V is presented where the regions of the highest current density can be localized.

When the NW is reverse biased at −1 V (Fig. 2(a) and (b)), the largest current density for the smaller NW radius of R_{ZnO}=12 nm is at least 5 orders of magnitude smaller than the largest current density for a radius of R_{ZnO}=30 nm. Local current crowding outside of the contact will occur when the area of the Au-ZnO interface is much smaller than the NW cross-sectional area that is supplying electrons where electrons concentrate at the edge region to maintain a constant flux. The area of high density current (~10^5 A/cm^2) will not contribute to the current transport through the contact due to a large potential barrier in the depletion region marked with black solid lines in Fig. 2(a) and (b). The current density at the metal-semiconductor interface will remain as low as ~10^{-4} A/cm^2 (Fig. 3(a)) but the current density at the contact edge will be increased by 2 orders of magnitude to ~10^{-2} A/cm^2 due to the large tunneling into the area of the local barrier thinning. This effect will be explained later.

At the forward bias of +1 V, a completely different electrical behavior is observed (Fig. 2(c) and (d)). At voltages higher than 0.2 V, the thermionic emission overtakes the tunneling current. This results in a uniform distribution of current through the NW structure and under the interface. The current density plot under the interface in Fig. 3(d) indicates a relatively higher current at the edge of the metal-semiconductor contacts in the corners of the higher electric field but the current density remains at the same order of magnitude through the whole length of the interface.

The schematic plot of the current vectors indicates the direction of current at −1 V (Fig. 3(b)) and +1 V (Fig. 3(e)). The highest current density area is indicated with longer vectors. When a forward bias is applied, the highest current density will be passing directly through the contact. It can be seen from the plot that, in reverse bias, the current is crowding ~3 nm away from the contact in the direction towards the contact, but only a very small current is passing directly through the contacts. This current crowding effect may lead to Joule heating which is known to result in heating or cooling near the contact area depending on the direction of the current flow [3]. It has been demonstrated that a large NW surface-to-volume ratio will lead to heat lost due to Joule heating of the semiconductor [25].

The result of the current calculations is shown in Fig. 3(c). A geometrical effect of the change in the NW radius results in a large Ohmic to Schottky behavior transformation in the current when the NW radius is reduced. At high forward bias, the current is caused by the thermionic emission. Due to high doping of the NW, the metal Fermi level will go above the conduction band and a significant increase in the current will be observed for both structure variations. At the reverse bias and small biases <0.2 V, the current will be dominated by tunneling due to the wide ZnO bandgap.

The microscale contact scaling will result in a reduced depletion width [26]. Leonard *et al.* [4] have shown that in the case of nanocontacts with the contact covering the entire end of Ge NWs, the depletion region width will be increased as the NW radius is scaled down. The black contour lines in Fig. 2(b) and (c) indicate the potential

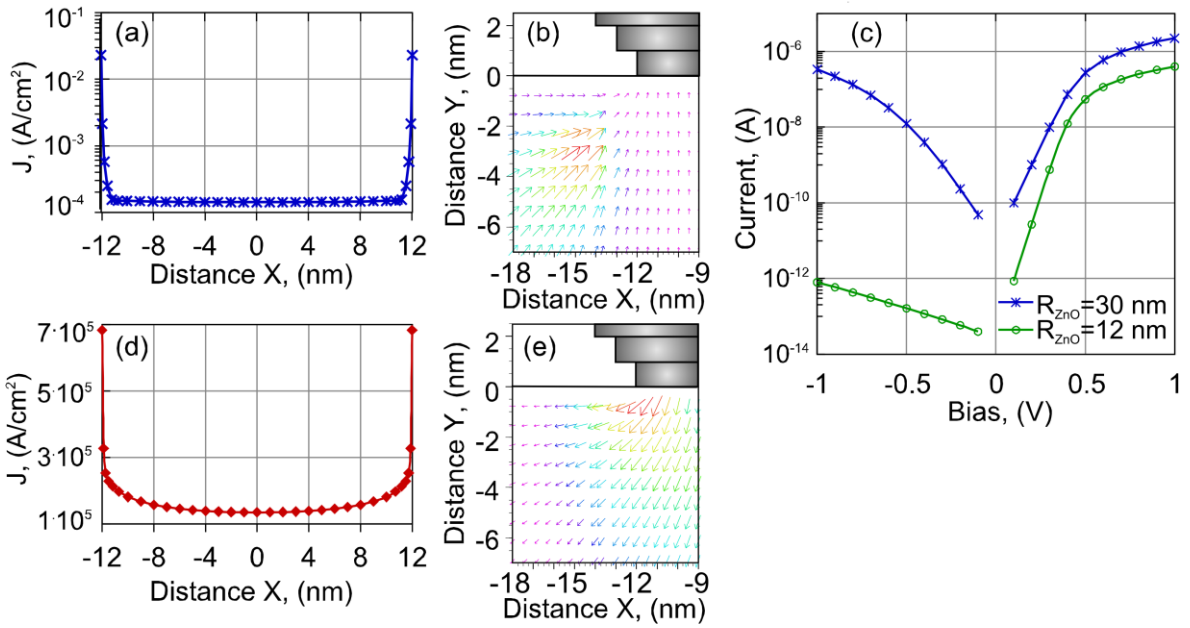

Fig. 3 Current density distribution directly under the contact interface at −1 V (a) and +1 V (d). The direction of the current flow near the contact is marked using vectors for −1 V (b) and +1 V (e). The regions of a larger current density are marked with the longer arrows. (e) I-V characteristics for both structure sizes of ZnO NW with R_{ZnO}=30 nm and R_{ZnO}=12 nm at a bias range from −1 V to +1 V.

distribution through the ZnO NW structure. It can be seen that the depth of the depletion region for the R_{ZnO}=12 nm radius is larger, which confirms that nanoscale contacts will have a complex behavior different from the behavior of microscale contacts. This effect will introduce a large potential barrier for the tunneling current in the case of the structure in Fig. 2(a) and will result in 4 orders of magnitude difference in the tunneling currents at reverse bias (Fig. 3(c)).

The tunneling current for the 15 nm contact will be additionally enhanced by the complex geometrical shape of the gold particle allowing a local thinning of the barrier shape at the edge of the contact (Fig. 2 (b)). This will lead to increase in the tunneling current and the main current transport will take place through a thin area of the contact edge.

A complex radial component of the current will be present in a contacted ZnO nanowire with a radius of R_{ZnO}=12 nm, indicating a vortex behavior[27] of the current in *x*- and *y*-directions at the forward and reverse biases. However, this radial current component will not significantly contribute to the total current density due to its low density.

Conclusion

In this work, we presented the influence of the contact geometry on the electrical properties of the end-bonded Schottky contact of ZnO nanowires with Au. For the Schottky contacts, the increase in the NW radius will lead to a parasitic effect of current crowding at reverse bias occurring at the edge of the contact away from the contact interface. Current crowding in forward bias will occur directly at the metal-semiconductor interface and this explains experimentally observed phenomena of metal contact melting in side-bonded Ohmic contacts of ZnO nanowires[13]. The Joule heating produced due to this effect might lead to a local breakdown of the contact, even though a large surface-to-volume ratio of the free-standing ZnO NW[25] and wide ZnO bandgap of the ZnO will reduce the heating. The simulations have demonstrated that a change in the geometry will also allow a change in the contact behavior without any adjustment to the material properties of the contact metal or semiconductor.

Acknowledgements

One of the authors (OK) would like to thank the Zienkiewicz Scholarship (Swansea University, UK) for financial support.

References

[1] Y. Chieh, A. Perera, J. Krusius, IEEE Trans. Electron Devices 39 (1992) 1882.
[2] A.D. Franklin, Z. Chen, Nat. Nanotechnol. 5 (2010) 858.
[3] K.L. Grosse, M.-H. Bae, F. Lian, E. Pop, W.P. King, Nat. Nanotechnol. 6 (2011) 287.
[4] F. Léonard, A. Talin, B. Swartzentruber, S. Picraux, Phys. Rev. Lett. 102 (2009).
[5] F. Léonard, a A. Talin, Nat. Nanotechnol. 6 (2011) 773.
[6] Y.W. Heo, D.P. Norton, L.C. Tien, Y. Kwon, B.S. Kang, F. Ren, S.J. Pearton, J.R. LaRoche, Mater. Sci. Eng. R Reports 47 (2004) 1.
[7] A. Kar, K.-B. Low, M. Oye, M. a. Stroscio, M. Dutta, A. Nicholls, M. Meyyappan, Nanoscale Res. Lett. 6 (2010) 3.
[8] M. Kirkham, X. Wang, Z.L. Wang, R.L. Snyder, Nanotechnology 18 (2007) 365304.
[9] A.M. Lord, T.G. Maffeis, A.S. Walton, D.M. Kepaptsoglou, Q.M. Ramasse, M.B. Ward, J. Köble, S.P. Wilks, Nanotechnology 24 (2013) 435706.
[10] M.M. Brewster, X. Zhou, S.K. Lim, S. Gradečak, J. Phys. Chem. Lett. 2 (2011) 586.
[11] Atlas User's Manual, 2007.
[12] R. Jackson, S. Graham, Appl. Phys. Lett. 94 (2009) 012109.
[13] S. LeBlanc, S. Phadke, T. Kodama, A. Salleo, K.E. Goodson, Appl. Phys. Lett. 100 (2012) 163105.
[14] E. Rhoderick, IEE Proc. I Solid State Electron Devices 129 (1982) 1.
[15] M. Aldegunde, S.P. Hepplestone, P. V Sushko, K. Kalna, Semicond. Sci. Technol. 29 (2014) 054003.
[16] G.D.J. Smit, S. Rogge, T.M. Klapwijk, Appl. Phys. Lett. 81 (2002) 3852.
[17] G.D.J. Smit, S. Rogge, T.M. Klapwijk, Appl. Phys. Lett. 80 (2002) 2568.
[18] W. Hong, J.I. Sohn, D. Hwang, S. Kwon, G. Jo, S. Song, S. Kim, H. Ko, S. Park, M.E. Welland, T. Lee, Nano Lett. (2008).
[19] S.M. Sze, K.K. Ng, Physics of Semiconductor Devices, Wiley, 2006.
[20] C.R. Crowell, S.M. Sze, Solid. State. Electron. 9 (1966) 1035.
[21] MeiKei Ieong, P.M. Solomon, S.E. Laux, H.-S.P. Wong, D. Chidambarrao, in:, Int. Electron Devices Meet. 1998. Tech. Dig. (Cat. No.98CH36217), IEEE, 1998, pp. 733–736.
[22] K. Matsuzawa, K. Uchida, a. Nishiyama, IEEE Trans. Electron Devices 47 (2000) 103.
[23] ATLAS Users Manual, Silvaco Inc., 2012.
[24] O. Kryvchenkova, R.J. Cobley, K. Kalna, Appl. Surf. Sci. 295 (2014) 173.
[25] F. Léonard, Appl. Phys. Lett. 98 (2011) 103101.
[26] G. Smit, S. Rogge, J. Caro, T. Klapwijk, Phys. Rev. B 69 (2004).
[27] J. Barker, A. Martinez, in:, Electr. Perform. Electron. Packag. IWCE-04, IEEE, 2004, pp. 215–216.